Catalytic and anticatalytic snapshots of a short-form ATP phosphoribosyltransferase

Magnus S. Alphey,[‡,¥] Gemma Fisher,[‡] Ying Ge,[¥] Eoin R. Gould,[¥] Teresa F. G. Machado, [¥] Huanting Liu,[¥] Gordon J. Florence,[¥] James H. Naismith,[¥,&,#,*] and Rafael G. da Silva[‡,*]

[‡]School of Biology and [¥]School of Chemistry, Biomedical Sciences Research Complex, University of St Andrews, St Andrews, Fife KY16 9ST UK

[&]Division of Structural Biology, University of Oxford, Oxford, OX3 7BN UK

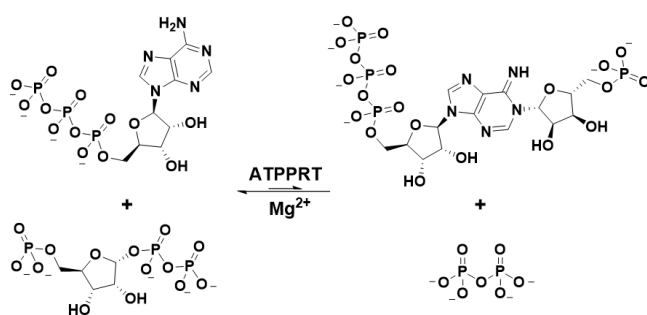[#]Research Complex at Harwell, Didcot, Oxon, OX11 0FA UK

*To whom correspondence may be addressed: rgds@st-andrews.ac.uk, phone: +44 01334 463496; naismith@strubi.ox.ac.uk

Abstract: Allosteric modulation of catalysis is a common regulatory strategy of flux-controlling biosynthetic enzymes. The enzyme ATP phosphoribosyltransferase (ATPPRT) catalyses the first reaction in histidine biosynthesis, the magnesium-dependent condensation of ATP and 5-phospho-α-D-ribosyl-1-pyrophosphate (PRPP) to generate N^1-(5-phospho-β-D-ribosyl)-ATP (PRATP) and pyrophosphate (PP_i). ATPPRT is allosterically inhibited by the final product of the pathway, histidine. Hetero-octameric ATPPRT consists of four catalytic subunits ($HisG_S$) and four regulatory subunits (HisZ) engaged in intricate catalytic regulation. HisZ enhances $HisG_S$ catalysis in the absence of histidine while mediating allosteric inhibition in its presence. Here we report $HisG_S$ structures for the apoenzyme and complexes with substrates (PRPP, PRPP-ATP, PRPP-ADP), product (PRATP), and inhibitor (AMP), along with ATPPRT holoenzyme structures in complexes with substrates (PRPP, PRPP-ATP, PRPP-ADP) and product (PRATP). These ten crystal structures provide an atomic view of the catalytic cycle and allosteric activation of *Psychrobacter arcticus* ATPPRT. In both ternary complexes with PRPP-ATP, the adenine ring is found in an anticatalytic orientation, rotated 180° from the catalytic rotamer. Arg32 interacts with phosphate groups of ATP and PRPP, bringing the substrates in proximity for catalysis. The negative charge repulsion is further attenuated by a magnesium ion sandwiched between the α- and β-phosphate groups of both substrates. HisZ binding to form the hetero-octamer brings $HisG_S$ subunits closer together in a tighter dimer in the Michaelis complex, which poises Arg56 from the adjacent $HisG_S$ molecule for cross-subunit stabilisation of the PP_i leaving group at the transition state. The more electrostatically pre-organised active site of the holoenzyme likely minimises the reorganisation energy required to accommodate the transition state. This provides a structural basis for allosteric activation in which chemistry is accelerated by facilitating leaving group departure.

Keywords: ATP phosphoribosyltransferase; allostery; HisG; HisZ; psychrophilic; catalytic activation; histidine biosynthesis

INTRODUCTION

Adenosine 5′-triphosphate phosphoribosyltransferase (ATPPRT) (EC 2.4.2.17) is a type-IV phosphoribosyltransferase (PRTase) in the PRTase superfamily.[1-2] ATPPRT is responsible for the first and flux-controlling step in histidine biosynthesis, the nucleophilic attack of adenosine 5′-triphosphate (ATP) N1 on 5-phospho-α-D-ribosyl-1-pyrophosphate (PRPP) C1 to generate N^1-(5-phospho-β-D-ribosyl)-ATP (PRATP) and inorganic pyrophosphate (PP$_i$)[3] (Scheme 1). The reaction is Mg^{2+}-dependent and reversible, with the equilibrium strongly favouring reactants.[4] ATPPRT is subjected to tight regulatory control in response to the metabolic status of the cell, being inhibited allosterically by histidine[3, 5] and orthosterically by AMP and ADP.[6] This enzyme is of interest as a potential drug target in some pathogenic bacteria,[1, 7-9] whilst in plants it is implicated in Ni^{2+}-tolerance,[10-11] and it is a model system for the study of allosteric modulation of catalysis.[7, 12-14]

Scheme 1. ATPPRT-catalysed nucleophilic substitution reaction.

The *hisG* gene encodes two forms of ATPPRT, a long-form of the protein (HisG$_L$) found in plants, fungi, and most bacteria,[13, 15] and a short-form (HisG$_S$) present in archaea and some bacteria.[16-17] HisG$_L$ is a homo-hexamer with each subunit consisting of two N-terminal domains containing the active site and a C-terminal allosteric domain responsible for histidine inhibition.[1] HisG$_S$ consists of two catalytic domains structurally similar to HisG$_L$'s, but lacks the C-terminal histidine-binding domain.[16-17] HisG$_S$ is found in complex with HisZ, a

catalytically inactive regulatory protein, the product of the *hisZ* gene, a paralog of histidyl-tRNA synthetase, forming the ATPPRT holoenzyme, a hetero-octamer where a HisZ tetramer is flanked by two $HisG_S$ dimers.[17-19] HisZ has a dual function: it allosterically enhances catalysis by $HisG_S$, and it binds histidine and therefore mediates allosteric inhibition.[17, 20]

Synthetic biology efforts have attempted to harness the histidine biosynthetic pathway for industrial production of histidine in bacteria,[21-23] as engineering of amino acid biosynthesis in microbes is a valuable tool for biocatalytic industrial production of these compounds.[24-25] An important challenge in exploitation is overcoming the strong inhibition of the pathway as histidine accumulates, with different strategies being employed towards that goal.[22-23] The recent discovery that $HisG_S$ is catalytically active in the absence of HisZ, while being insensitive to histidine,[15, 18] opens the possibility of utilising this enzyme as a starting point for biotechnological production of histidine. However, significant activity is lost in the absence of HisZ.[15, 18] Elucidating the catalytic mechanism of $HisG_S$ could aid in rational engineering of a fully active $HisG_S$ for histidine production.

In the present work, we report ten crystal structures of the psychrophilic bacterium *Psychrobacter arcticus* $HisG_S$ (*Pa*$HisG_S$) and ATPPRT holoenzyme (*Pa*ATPPRT) bound to substrates, product and inhibitor. Two of the structures contain both PRPP and ATP in the active site, providing a rare glimpse of the pre-catalytic ternary complex. Analysis of the structures, along with site-directed mutagenesis, uncovers the basis for allosteric activation and allows a catalytic mechanism to be proposed.

MATERIALS AND METHODS

Materials. ATP, PRPP, ribose, $MgCl_2$, deuterium oxide (99.9 atom % deuterium), tricine, triethylamine, acetic acid, dithiothreitol (DTT), imidazole, glycerol, lysozyme, DNAse I, ampicillin, kanamycin, and chloramphenicol were purchased from Sigma-Aldrich. EDTA-

4

free Cømplete protease inhibitor cocktail was from Roche. Isopropyl-β-D-1-thiogalactopyranoside was purchased from Fisher Scientific. All other chemicals were purchased from readily available commercial sources, and all were used without further purification. *Pa*HisG$_S$, *P. arcticus* HisZ (*Pa*HisZ), *Mycobacterium tuberculosis* pyrophosphatase (*Mt*PPase), and tobacco etch virus protease were obtained as previously published.[18] *Escherichia coli* PRPP synthetase (*Ec*PRPPS) cloning, expression and purification, synthesis of D-ribose 5-phosphate, and synthesis and purification of PRATP are described in the Supporting Information.

Crystallisation of PaATPPRT. Crystals of *Pa*ATPPRT were obtained at 4 °C as previously described.[18] To obtain structures of the complexes with various ligands (PRPP, PRPP + ATP, PRPP + ADP, PRATP), crystals were washed in buffer containing 10% polyethylene glycol (PEG) 3350, 0.1 M bicine pH 8.5, 50 mM MgCl$_2$, 0.1 M KBr, 4% 1,6-hexanediol, then transferred to a 1-μL drop of this solution in which solid ligands soaked for 30 s − 12 h. For data collection, crystals were transferred to a fresh drop of soaking solution substituted with 20% 2-methyl-2,4-pentanediol (MPD) for 10 s then flash-cooled in a stream of nitrogen gas at 100 K.

Crystallisation of PaHisG$_S$. Crystals were grown and handled at 4 °C as follows. *Pa*HisG$_S$ in buffer containing 20 mM Tris HCl pH 8.0, 50 mM KCl, 10 mM MgCl$_2$, and 2 mM DTT was concentrated to 10 mg mL^{-1}. Crystallization screens were performed with commercially available and in-house stochastic screens. Hanging drops (150 nL protein solution and 150 nL of screen solution) were set up using an ArtRobbins Gryphon crystallization robot. One in-house condition gave small cube-shaped crystals with dimensions 0.05 x 0.05 x 0.03 mm^3. The precipitant solution contained 34% PEG 3350, 0.1 M MOPS pH 6.5, 0.1 M K/Na tartrate. Crystals were reproduced by seeding into sitting and hanging drops

of protein with mother liquor containing 32% PEG 3350, 0.1 M MOPS pH 6.5, 0.1 M K/Na tartrate. Thin plate-like crystals grew in 3 weeks to a size suitable for data collection. To prepare ligand complexes (PRPP, PRPP + ATP, PRPP + ADP, PRATP, AMP), crystals were soaked in a drop containing 34% PEG 3350, 0.1 M bicine pH 8.5, 0.1 M K/Na tartrate, and 20 mM MgCl$_2$ to which solid ligand had been added. Crystals were soaked for 3 – 24 h then cryoprotected with 20% MPD and frozen at 100 K for data collection. The apoenzyme and PRPP-ATP complex were also soaked in the presence of 22% glycerol with no differences observed in the final structures.

X-ray data collection and processing. X-ray diffraction data were collected either in-house as previously[18] reported or at the Diamond Light Source, Oxfordshire, UK. Data were processed either in-house using iMosflm[26] or the automated processing pipeline at Diamond with Xia2[27] integrated with XDS[28]. Data collection statistics are shown in Tables S1 and S2. The ligand-bound structures of *Pa*ATPPRT were solved by molecular replacement with MOLREP[29] using 5M8H[18] as search model. The apo and ligand-bound structures of *Pa*HisG$_S$ were solved by molecular replacement using 5M8H[18] chain E as search model. Structures were refined using cycles of model building with COOT[30] and refinement with Refmac[31]. The electron density in the omit map showed the presence of ligands in each of *Pa*HisG$_S$ active sites though the occupancy was not always 100%. In the apo-structure, some electron density was observed in the active site and modelled as tartrate, present in the soaking solution. Additional electron density was observed in *Pa*ATPPRT complexes with PRPP-ATP and with PRATP, and was modelled as Tris, the buffer in which the proteins were solubilised. ATP and ADP library files were generated with AceDRG.[32] The coordinate and library files for PRATP were generated using PRODRG[33]. Refinement statistics are shown in Tables S1 and S2 for *Pa*HisG$_S$ and *Pa*ATPPRT structures, respectively. All coordinates and structure factor files

6

have been deposited in the Protein Data Bank, and the corresponding PDB ID's are shown in Tables S1 and S2.

Determination of PaHisG$_S$ quaternary structure in solution. *Pa*HisG$_S$ (3.3 mg) was subjected to size-exclusion chromatography (SEC) on a HiLoad 16/600 Superdex 200 pg column (GE healthcare) equilibrated with 20 mM HEPES pH 8.0. The sample was eluted in the same buffer at a flow rate of 1 mL min^{-1}. The eluate was analyzed by multi-angle light scattering (MALS) detector DAWN HELEOS-II and refractive index detector Optilab T-rEX (Wyatt Techonologies). The elution peak, shown as changes in refractive index, was divided into 1-mL fractions in the ASTRA 6.1 software (Wyatt Techonologies) for calculations of molecule size in mean square radius (nm²) and molecular mass.

Site-directed mutagenesis of PaHisG$_S$. Replacement of arginine for alanine at position 56 of *Pa*HisG$_S$ was accomplished by the method of Liu and Naismith,[34] with primers 5′-GCGCTAAGCTGATCTTCCCGACCAGCAACCCTAATGTG-3′ and 5′-GGAAGATCAGCTTAGCGCTCGCTTCCGGATCTTCCAGC-3′. Successful mutation was confirmed by DNA sequencing (Eurofins Genomics). R56A-*Pa*HisG$_S$ was expressed and purified by the same protocol reported for wild-type (WT) *Pa*HisG$_S$.[18] Trypsin-digestion of R56A-*Pa*HisG$_S$ followed by ESI-MS/MS analysis of the tryptic peptides further confirmed the presence of the mutation at position 56. Both WT- and R56A-*Pa*HisG$_S$ at various concentrations were assayed for catalytic activity under initial-rate condition at 20 °C in the presence of 5.6 mM ATP and 2 mM PRPP and in the presence or absence of 17 μM *Pa*HisZ, along with other reaction components as previously described,[18] in a Shimadzu UV-2600 spectrophotometer. Measurements were carried out in duplicate.

RESULTS AND DISCUSSION

PRATP production. HPLC purification of PRATP is shown in Figure S1A. ESI-MS analysis showed the expected mass of 718.0 (Figure S1A inset), and the ^{31}P-NMR spectrum (Figure S1B) displayed chemical shifts identical to those previously assigned.[18]

Crystal structures of apo, PRPP-, PRPP-ATP-, and PRATP-bound PaHisG$_S$. To gain insight into catalysis, *Pa*HisG$_S$ crystal structures were solved in apo form and in complex with substrates and product. *Pa*HisG$_S$ crystallised in I2 space group, and refinement statistics are summarised in Table S1. There is one monomer in the asymmetric unit, with a homodimer formed by crystallographic symmetry. Subunits in the homodimer interact in a head-to-tail arrangement (Figure S2A and B) almost identical to the arrangement found in the *Pa*ATPPRT structure.[18] SEC-MALS analysis was used to establish the quaternary structure of *Pa*HisG$_S$ in solution (Figure S3), resulting in a calculated molecular mass of *ca.* 48000, consistent with a homodimer (the monomer mass is 25215). This is the same oligomeric state reported for *Lactococcus lactis* HisG$_S$.[15] Experimental density maps for all ligands are shown in Figure S2C. Overlaying Cα atoms among the four structures resulted in root-mean-square deviations (rmsd) of 0.26 Å, 0.22 Å, and 0.13 Å between *Pa*HisG$_S$ and *Pa*HisG$_S$-PRPP, *Pa*HisG$_S$-PRPP and *Pa*HisG$_S$-PRPP-ATP, and *Pa*HisG$_S$-PRPP-ATP and *Pa*HisG$_S$-PRATP, respectively (Figure 1), reflecting minimal changes in overall subunit structure upon binding of substrates and product.
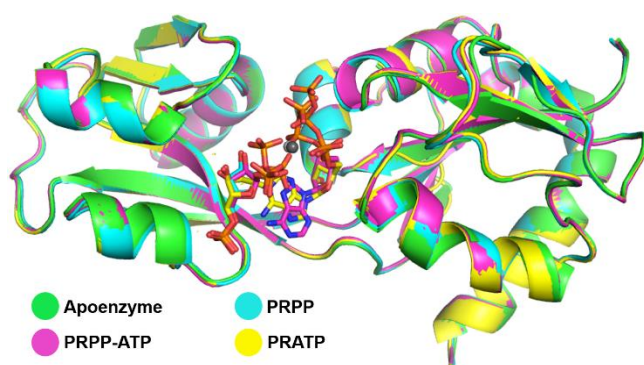

● Apoenzyme   ● PRPP
● PRPP-ATP   ● PRATP

Figure 1. Ribbon diagram of the overlay of apo, PRPP-, PRPP-ATP-, and PRATP-bound *Pa*HisG$_S$ subunits. Ligands are represented as stick models with carbon coloured as the corresponding ribbon, nitrogen in blue, oxygen in red, and phosphorus in orange. Magnesium ions are shown as light and dark grey spheres in the ATP-PRPP and PRATP structures, respectively.

*Pa*HisG$_S$ *active site*. Structures of *Pa*HisG$_S$-PRPP, *Pa*HisG$_S$-PRPP-ATP, and *Pa*HisG$_S$-PRATP complexes show clear electron density for the ligands (Figure 2A-C) and reveal significant differences in active site interactions in comparison with other ATPPRT's.[8, 13, 19, 35-36] Table S3 compiles key information on all structures of ATPPRT published to date, including the ones from this work. In the *Pa*HisG$_S$-PRPP structure, the substrate is anchored to the active site via several polar contacts among the 5-PO$_4$$^{2-}$ group and main-chain and side-chain atoms in the PRPP-binding loop (residues 179 to 183), and a hydrogen bond (H-bond) between the 2-OH group and Asp176 side chain (Figure 2D). This H-bond prevents PRPP from obstructing the ATP-binding site, indicating a catalytically viable binary complex, similar to that seen in the *L. lactis* ATPPRT-PRPP structure,[19] but contrary to the complex between PRPP and the *Campylobacter jejuni* ATPPRT structure.[36] The PP$_i$ moiety of PRPP appears to be more flexible (B-factors between 68 and 83) than the 5-phosphoribosyl moiety (B-factors between 23 and 45). The increased flexibility is consistent with the lack of specific contacts with the protein. Its only interaction is with a water molecule that also interacts with the 5-phosphoribosyl (Figure 2D). In the *L. lactis* ATPPRT-PRPP, a serine residue side chain donates an H-bond to the α-PO$_4$$^{2-}$ of the PP$_i$ moiety of PRPP.[19] Mutations in conserved residues (T159A and T162A) in the PRPP-binding loop in *L. lactis* ATPPRT had detrimental effect on PRPP binding, but little influence on the catalytic rate.[35]

9

Despite numerous attempts involving both soaking and co-crystallisation, the *Pa*HisG$_S$-ATP binary complex structure could not be obtained. On the other hand, the structure of the Michaelis complex with both PRPP and ATP bound to *Pa*HisG$_S$ was readily attained (Figure 2B), the first structure of an ATPPRT with both substrates in the active site. PRPP sits in a similar orientation in the ternary complex as it does in the binary (Figure 2D and E). Upon ATP binding, Arg32 side chain rotates *ca.* 180° around its Cγ-Cδ axis, breaking its H-bond with Asp179, to position its guanidinium group parallel to the adenine ring (Figure 2E). An Arg32-Asp179 salt bridge in the *Pa*HisG$_S$-PRPP binary complex holds the active site open, otherwise Arg32 would prevent ATP binding (Figure 2E). A similar position of the equivalent arginine is found in the *C. jejuni* ATPPRT-ATP structure,[13] and the residue is conserved in ATPPRT's (Figure S4). Asp94 accepts H-bonds from the 2′- and 3′-OH groups, as in *C. jejuni* and *M. tuberculosis* ATPPRT complexes with ATP,[8, 13] and Lys137 forms a salt bridge with the β-PO$_4^{2-}$. ATP binding is further stabilised by a salt bridge between its γ-PO$_4^{2-}$ and Arg73 from the adjacent subunit (Figure 2E). The importance of this interaction may be negligible, though. The equivalent position in *L. lactis* ATPPRT is Lys50 which likely participates in a similar salt-bridge, but the K50A mutant has only moderate effect on ATP binding and catalysis.[35]
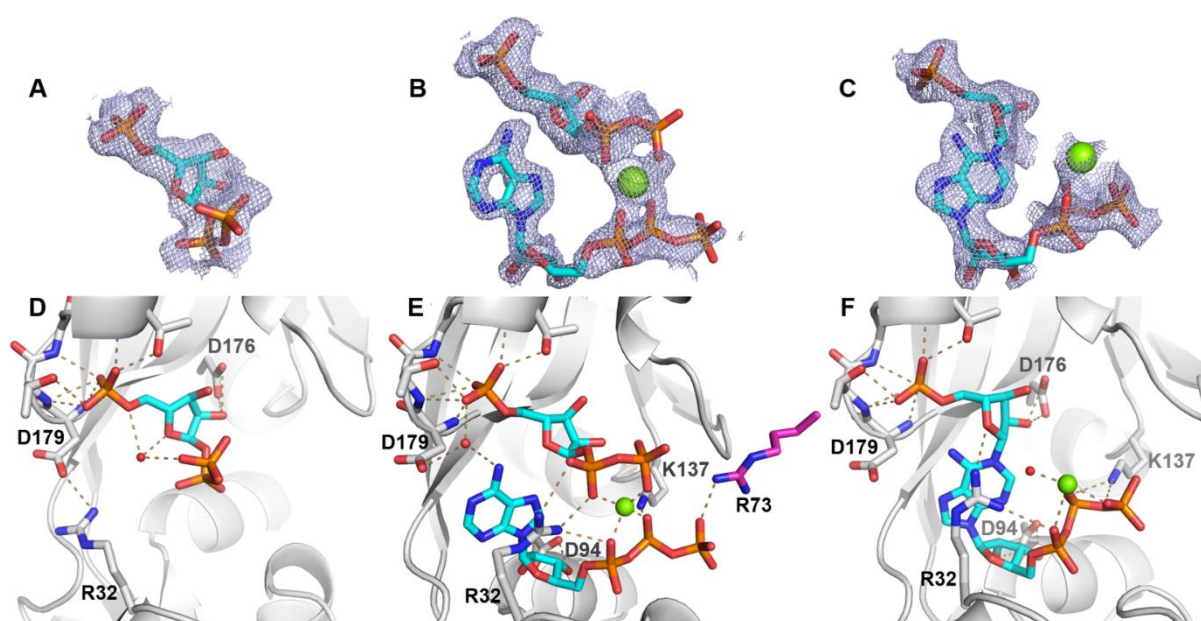
Figure 2. *Pa*HisG_S structures in complex with substrates and product. (A) PRPP, (B) PRPP-ATP, and (C) PRATP omit maps at 1.0σ. Active-site close-up of *Pa*HisG_S bound to (D) PRPP, (E) PRPP-ATP, and (F) PRATP. In A-F, magnesium and waters are shown as green and red spheres, respectively, while ligands are represented as stick models with carbon in cyan, nitrogen in blue, oxygen in red, and phosphorus in orange. In D-F, the protein backbone is shown as ribbon diagram, with selected residues' main and side chains shown as stick models coloured as the ligands except that carbon is in grey (same subunit) or magenta (adjacent subunit). Polar interactions are depicted by dashed lines.

ATP and PRPP are brought into proximity for catalysis by salt bridges between Arg32 and α-PO_4^{2-} groups of both substrates, and electrostatic repulsion among the negatively charged phosphate groups is attenuated by a Mg^{2+} ion sandwiched between the α- and β-PO_4^{2-} groups of both PRPP and ATP, presumably the origin of the divalent metal requirement for catalysis. Except for Arg32, no other residue in the dimer interacts directly with the PP_i moiety of PRPP, but its β-PO_4^{2-} accepts an intramolecular H-bond from the 2-OH group (Figure 2E). Given this scarcity of contacts with the enzyme, one might speculate that a second Mg^{2+} ion be necessary to stabilise the PP_i leaving group at the transition state, since PP_i's departure as leaving group often involves a Mg^{2+} complex in enzymatic reactions,[37] but its interaction with PRPP in the Michaelis complex might not be stable enough to be captured in the crystal structure. Absence of a putative second Mg^{2+} ion notwithstanding, catalysis would be prevented here owing to the orientation of the adenine, which places the nucleophile N1 away from PRPP C1. This orientation is held in place by a water-mediated interaction among Asp179, ATP 6-NH_2 and PRPP 5-PO_4^{2-} (Figure 2E). This anticatalytic ATP rotamer found in the structure is a possible reason a complex with both substrates could be trapped in the first place, since the catalytically active wild-type enzyme was used for crystallisation. Another

likely contributing reason is the reaction equilibrium, which strongly favours the reactants.[4] For the nucleophilic attack of ATP N1 on PRPP C1 to occur, the adenine must rotate *ca.* 180° around the N9-C1′ axis. In solution, thermal motion-driven conformational flexibility of the Michaelis complex would permit the stochastic sampling of reactive adenine orientations, but such flexibility is likely to be restrained in *Pa*HisG$_S$ crystals. This hypothesis is further supported by the *C. jejuni* ATPPRT-ATP structure, where electron density for both rotamers was reported.[13]

The structure of *Pa*HisG$_S$-PRATP binary complex shows electron density for the entire product (Figure 2C), as in the recent *C. jejuni* ATPPRT structure.[36] Most interactions between enzyme and ligands found in the *Pa*HisG$_S$-PRPP and *Pa*HisG$_S$-PRPP-ATP structures are retained in the *Pa*HisG$_S$-PRATP complex, and the Mg^{2+} ion is coordinated to the α-, β-, and γ-PO$_4^{2-}$ of the product (Figure 2F). Overlay of the ligands in the three structures shows remarkably similar positions for the phosphoribosyl and triphosphoribosyl moieties and the Mg^{2+} ions in all structures (Figure 3). An interesting observation in the *Pa*HisG$_S$-PRATP structure is the 1.6-Å movement of one of the η-NH groups of Arg32 towards the PRPP-binding site, maintaining the guanidinium plane parallel to the adenine, but now donating an H-bond to the O4″ of PRATP (Figure 2F). This interaction might have mechanistic consequences, as it would further polarise the O4″-C1″ (product numbering) bond, increasing C1″ electrophilicity, making it more prone to nucleophilic attack in an A$_N$D$_N$ mechanism.[38-39] However, in a D$_N$*A$_N^{\ddagger}$ mechanism,[38] as proposed for other ATPPRT's based on kinetic isotope effects,[8] this interaction would be detrimental since it would destabilise the ribooxocarbenium ion intermediate. This raises the possibility that the *Pa*HisG$_S$-catalysed reaction proceeds via a different transition state.
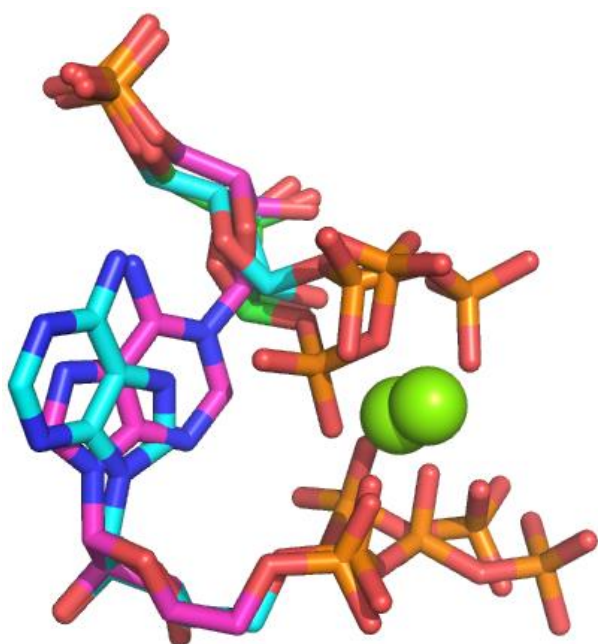
Figure 3. Overlay of *Pa*HisG$_S$-bound ligands PRPP, PRPP-ATP, and PRATP structures. Magnesium is shown as sphere (green) while molecules are shown as stick with nitrogen in blue, oxygen in red, phosphorus in orange, and carbon in green (PRPP), cyan (PRPP-ATP), and magenta (PRATP).

Crystal structures of AMP- and PRPP-ADP-bound PaHisG$_S$. AMP and ADP are competitive inhibitors of HisG$_L$ ATPPRT's with respect to both ATP and PRPP, providing an additional regulatory check-point that reflects the metabolic state of the cell.[6, 35] This is explained structurally by the fact that the 5′-phosphorybosyl and adenine moieties of AMP span the 5′-phosphoribosyl and adenine binding sites of PRPP and ATP, respectively.[1-2, 13] The *Pa*HisG$_S$-AMP structure (Figure 4A) shows the same overall binding mode for AMP as in other ATPPRT's.[1-2, 13] The 5′-PO$_4^{2-}$ group makes similar interactions with the protein as the corresponding group in PRPP does. The adenine is anchored via H-bonds donated by its 6-NH$_2$ group to Ala113 α-carbonyl oxygen and Arg32 guanidinium, and by an H-bond between its N7 and Arg32 guanidinium (Figure 4B).
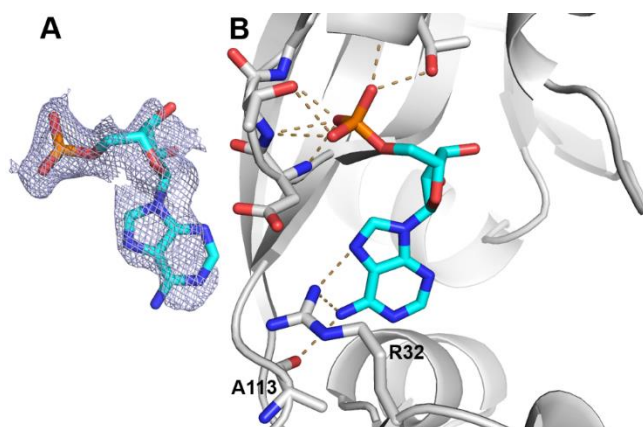
13

Figure 4. *Pa*HisG$_S$ structure in complex with AMP. (A) AMP omit map at 1.0σ. (B) Active-site close-up of *Pa*HisG$_S$ bound to AMP. In A and B, ligands are represented as stick models with carbon in cyan, nitrogen in blue, oxygen in red, and phosphorus in orange. In B, the protein backbone is shown as ribbon diagram, with selected residues' main and side chains shown as stick models coloured as the ligands except that carbon is in grey. Polar interactions are depicted by dashed lines.

Crystals of the *Pa*HisG$_S$-ADP binary complex could not be obtained, as was the case with ATP, but the structure of the *Pa*HisG$_S$-PRPP-ADP ternary complex was readily determined (Figure 5A). ADP sits in the active site in same way ATP does, and almost all interactions present in the *Pa*HisG$_S$-PRPP-ATP complex (Figure 2E) are preserved in the *Pa*HisG$_S$-PRPP-ADP structure, including the Mg^{2+} ion binding between the α- and β-PO$_4^{2-}$ groups of both ligands (Figure 5B). An exception is the salt bridge with Arg73 of the adjacent subunit. This residue is found in the same position as in the ATP-PRPP complex, but it is too far away to reach the β-PO$_4^{2-}$ of ADP. Overlay of the ligands in these two structures shows hardly any difference in binding (Figure 5C). This suggests that ADP is not an inhibitor of *Pa*HisG$_S$, but may be an alternative substrate.
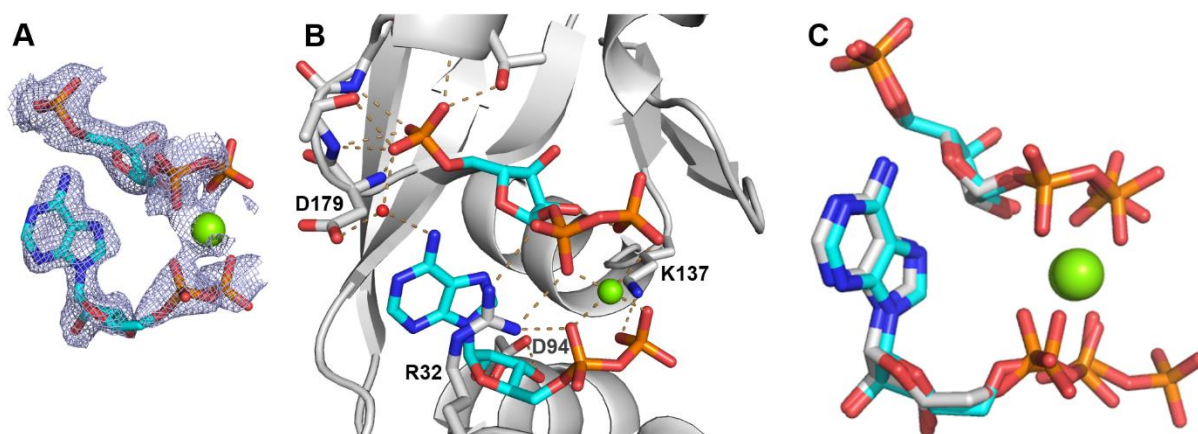
Figure 5. Structure of *Pa*HisG$_S$-PRPP-ADP complex. (A) PRPP-ADP omit map at 1.0σ. (B) Active-site close-up of *Pa*HisG$_S$ bound to PRPP-ADP. (C) Overlay of PRPP-ATP and PRPP-ADP structures. In A and B, magnesium and waters are shown as green and red spheres, respectively, while ligands are represented as stick models with carbon in cyan, nitrogen in blue, oxygen in red, and phosphorus in orange. The protein backbone is shown as ribbon diagram, with selected residues' main and side chains shown as stick models coloured as the ligands except that carbon is in grey. Polar interactions are depicted by dashed lines. In C, colours are the same as in A and B, except that carbon is in cyan for PRPP-ATP and grey for PRPP-ADP.

Crystal structures of PRPP-, PRPP-ATP-, PRATP-, and PRPP-ADP-bound PaATPPRT. It is well known that HisG$_S$ catalysis is activated by HisZ,[15, 18, 20] but the mechanism of activation is still elusive. We have recently published the structure of *Pa*ATPPRT apoenzyme,[18] and to uncover structural features that could account for activation and to glean further information on catalysis, *Pa*ATPPRT structures were solved in complex with PRPP, PRPP-ATP, PRATP and PRPP-ADP, and refinement statistics are summarised in Table S2. *Pa*ATPPRT-PRPP crystallised in the P2$_1$ space group with one full hetero-octamer in the asymmetric unit (Figure 6A), as found for apo *Pa*ATPPRT.[18] The remaining structures were solved in the C2 space group and had a *Pa*HisG$_S$ dimer and a *Pa*HisZ dimer in the

asymmetric unit (Figure 6B), with the hetero-octamer formed by crystallographic symmetry. Experimental and refined electron density maps for all ligands are shown in Figure S5. The position of the Mg^{2+} ion in the PRATP structure could not be unambiguously assigned.
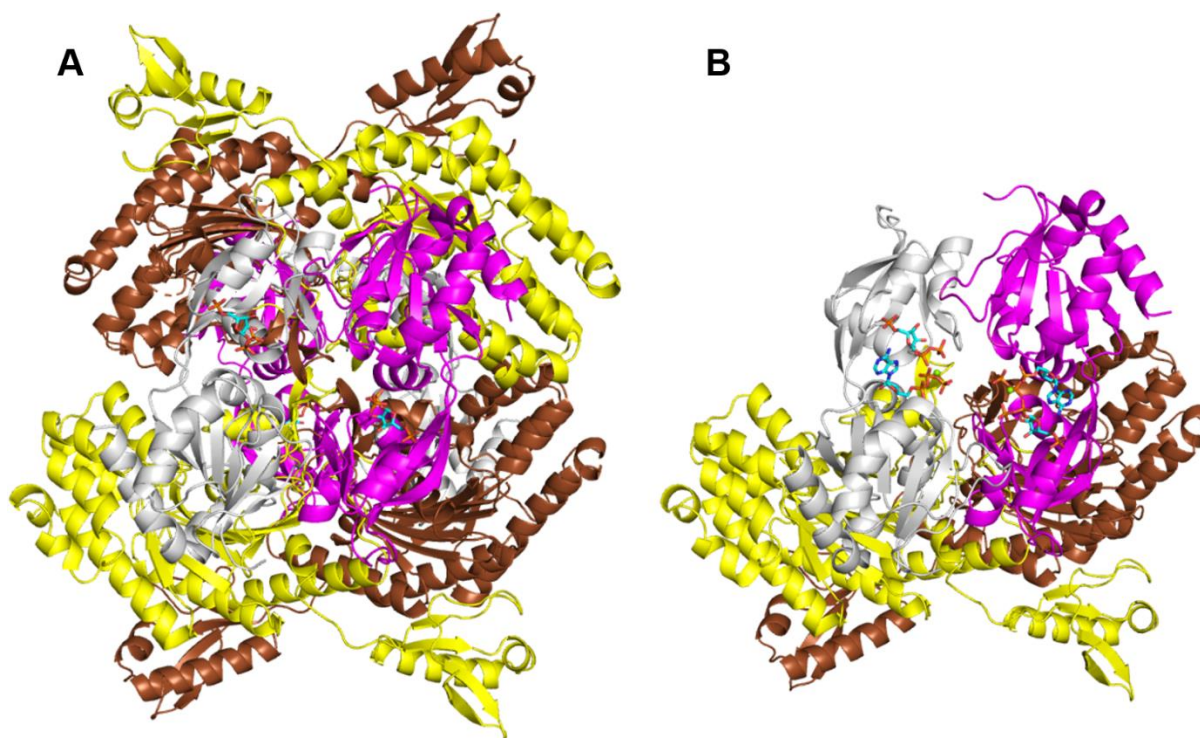

Figure 6. Ribbon diagrams of *Pa*ATPPRT structures with bound (A) PRPP and (B) PRPP-ATP. *Pa*HisG$_S$ subunits are shown in grey and magenta, while *Pa*HisZ subunits are shown in yellow and brown. Magnesium is shown as sphere (green) while substrates are shown as stick with nitrogen in blue, oxygen in red, phosphorus in orange, and carbon in cyan.

PaATPPRT active site. Most interactions between protein and ligands present in the *Pa*HisG$_S$ structures are retained in the corresponding *Pa*ATPPRT, with some additional ones (Figure 7). In the PRPP- and PRPP-ATP-bound structures, Glu163 accepts an H-bond from the 3-OH group, which may help position PRPP for catalysis (Figure 7A and B). The adjacent *Pa*HisG$_S$ subunit contributes two residues to the active site, Arg56 and Arg73. The side chain of Arg73 anchors the γ-PO_4^{2-} in the ternary complex, as seen in the *Pa*HisG$_S$ structure, and its position changes little from the substrate and product binary complexes. The equivalent residue

16

is conserved in *T. maritima* ATPPRT,[17] and is replaced by a lysine in the *L. lactis* enzyme.[20] Most revealing in all three structures is the position of Arg56. This residue is in the middle of a flexible loop extending residues Ala44-Val67, and its guanidium group lies *ca.* 12 Å away from the PRPP β-PO$_4^{2-}$ in the binary complex. Upon ATP binding, Arg56 side chain moves towards the active site to form a salt bridge with the PP$_i$ moiety of PRPP (Figure 7B). This interaction is responsible for leaving group stabilisation during the transition state, possibly aided by a putative second Mg^{2+} ion as PP$_i$ likely departs the enzyme as a Mg^{2+} complex. In the PRATP complex (Figure 7C), Arg56 is more than 6 Å away from its position in the ternary complex. Amino acid multiple sequence alignment of HisG$_S$'s reveals the high degree of conservation of this residue (Figure S4), lending support to its role in catalysis.
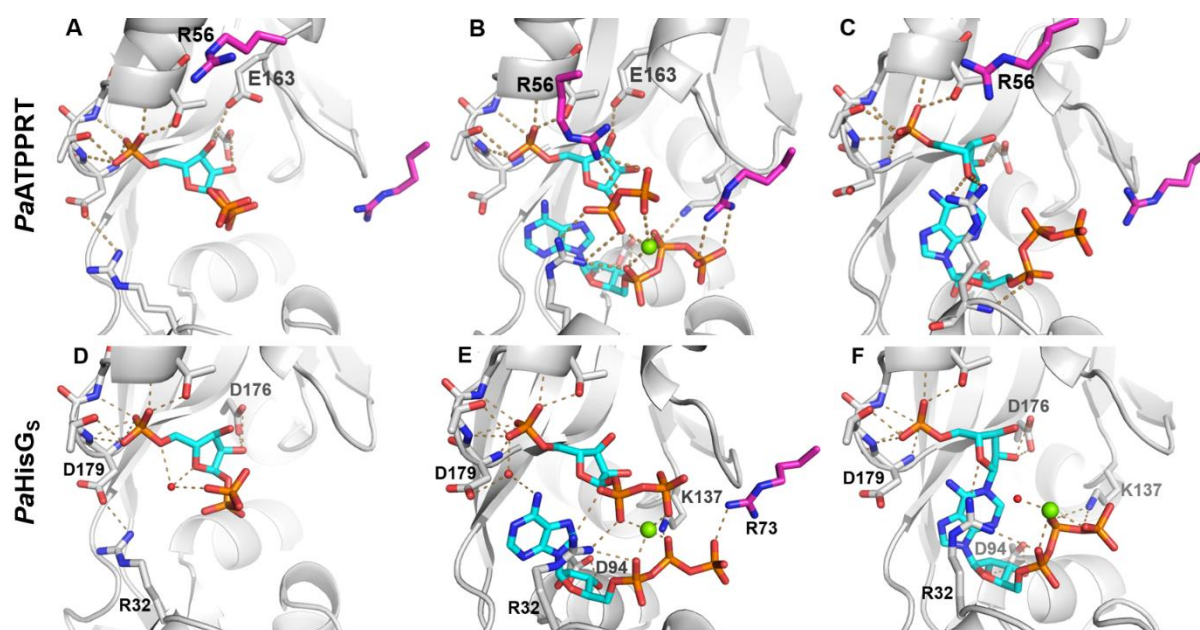

Figure 7. Active-site close-up of *Pa*ATPPRT bound to (A) PRPP, (B) PRPP-ATP, and (C) PRATP, compared with the corresponding structures in *Pa*HisG$_S$ (D – F). Magnesium is shown as green sphere while ligands are represented as stick models with carbon in cyan, nitrogen in blue, oxygen in red, and phosphorus in orange. The protein backbone is shown as ribbon diagram, with selected residues' main and side chains shown as stick models coloured as the

ligands except that carbon is in grey. The side chains of two Arg residues contributed by the adjacent subunit are shown as stick models coloured as the ligands except that carbon is in magenta. Only residues whose interactions with ligands are absent in the PaHisG$_S$ structures (D – F) are labelled in the PaATPPRT structures (A – C). Polar interactions are depicted by dashed lines.

Contacts in the PaATPPRT-PRPP-ADP structure (Figure S6) are similar to those in PaHisG$_S$. This is consistent with ADP acting as a substrate for this enzyme, contrary to its inhibitory role in HisG$_L$ ATPPRT's.[6] The adenine ring in the two PaATPPRT Michaelis complexes is found in the same anticatalytic orientation seen in the corresponding PaHisG$_S$.

Structural basis of allosteric activation. PaHisZ has little effect on the overall structures of PaHisG$_S$ apoenzyme and PRPP- and PRATP-bound binary complexes, as evidenced by superposition of Cα atoms of these forms of PaHisG$_S$ dimers onto their counterparts in PaATPPRT (Figure S7), resulting in rmsd's of 0.41 Å, 0.47 Å, and 0.40 Å, respectively. However, overlay of Cα atoms of PaHisG$_S$ dimers in complex with PRPP-ATP with and without PaHisZ show the catalytic subunits moving closer to one another upon binding of the regulatory protein (Figure 8A), yielding an rmsd of 1.49 Å. This affects cross dimer contacts of specific side chains with substrates. While Arg73 position is very similar in PaHisG$_S$ and PaATPPRT and maintains is interaction with the γ-PO$_4^{2-}$ of the adjacent subunit, Arg56 position changes drastically in the two enzymes, and only forms a salt bridge with the PP$_i$ moiety of PRPP in the PaATPPRT structure (Figure 8B). In nonactivated PaHisG$_S$ ternary complex, Arg56 side chain lies over 7 Å away from the PP$_i$ moiety of PRPP. Given that Arg56 is the most likely candidate to stabilise the leaving group in the chemical step, catalysis is favoured in PaATPPRT owing to its ability to respond more readily to ternary-complex formation than PaHisG$_S$. A more electrostatically pre-organised active site in the holoenzyme

18

incurs in lower reorganisation energy penalty as the Michaelis complex moves towards the transition state where a highly charged leaving group must be stabilised.[40-41] It should be pointed out that even though our hypothesis for the structural features underlying allosteric activation is based on static snapshots, it is entirely compatible with a contemporary view of allostery and catalysis that reflects the dynamic fluctuation of the enzyme across the conformational space,[12, 42-43] with the catalytically favourable position of Arg56 stochastically sampled more often in *Pa*ATPPRT than in *Pa*HisG$_S$.
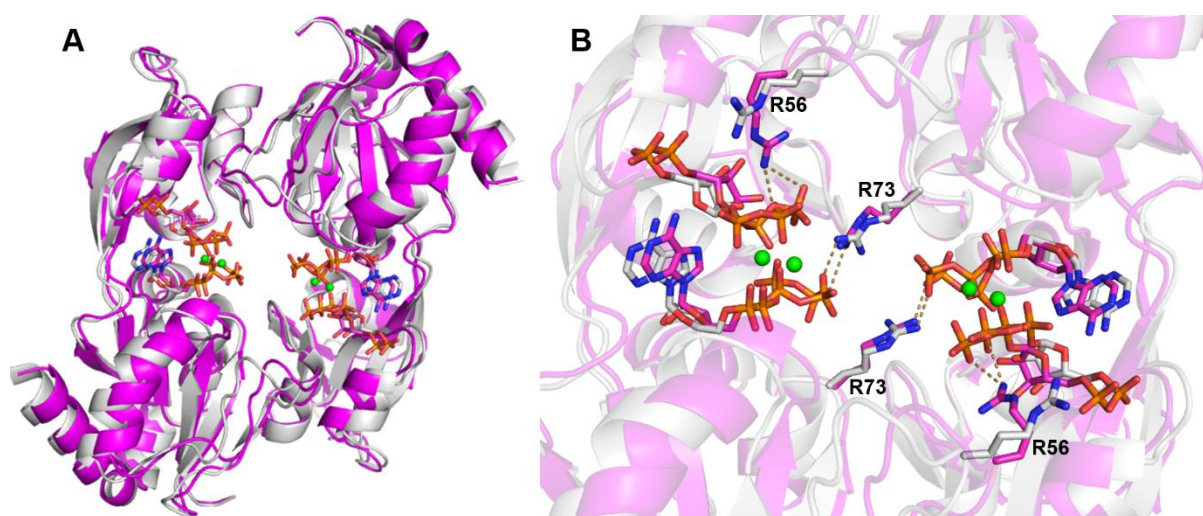

Figure 8. *Pa*HisZ-induced active site pre-organisation in *Pa*ATPPRT. (A) Overlay of PRPP-ATP-bound *Pa*ATPPRT (magenta) and *Pa*HisG$_S$ (grey) dimers. (B) Active site close-up of the superimposed dimers showing cross-subunit contacts. Magnesium ions are shown as green spheres while substrates, Arg56 and Arg73 side chains are represented as stick models with nitrogen in blue, oxygen in red, phosphorus in orange, and carbon in magenta (*Pa*ATPPRT) and grey (*Pa*HisG$_S$). Polar interactions are depicted by dashed lines.
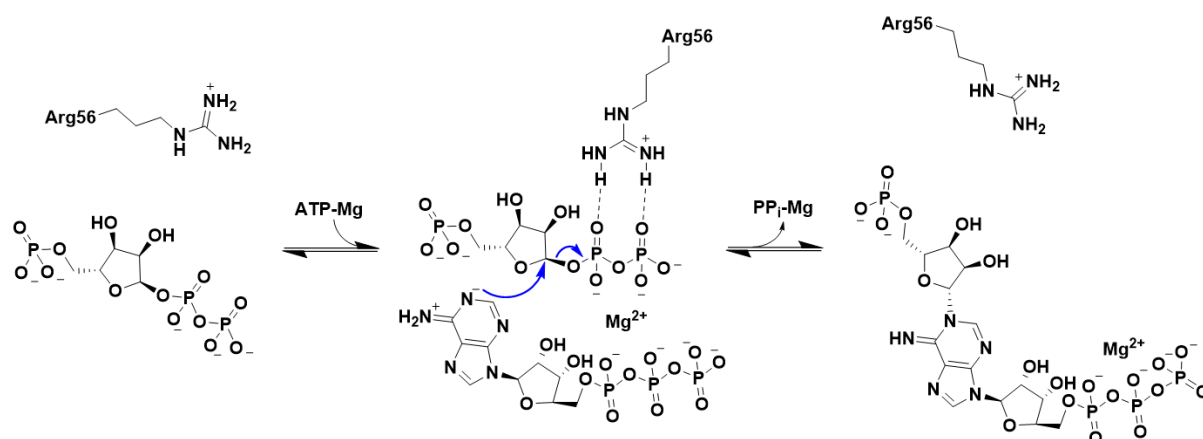
Effect of Arg56Ala mutation on catalysis. The crystal structures suggest that Arg56 plays a key role in catalysis by stabilising the leaving group. To test that hypothesis, the enzymatic activities of R56A-*Pa*HisG$_S$ and WT-*Pa*HisG$_S$ were evaluated with and without *Pa*HisZ (Figure S8). Upon correction for enzyme concentration, in the absence of *Pa*HisZ,

R56A-PaHisG$_S$ reaction rate is 86-fold lower than that of WT-PaHisG$_S$, evidencing a crucial role in catalysis for Arg56. Interestingly, in the presence of PaHisZ, R56A-PaHisG$_S$ reaction rate is 6-fold lower than that of the WT-PaHisG$_S$ (Figure S8B). This suggests that, while Arg56 still plays an important role in PaATPPRT catalysis, the activated enzyme promotes sampling of different conformations that potentially positions another residue to stabilise the leaving group PP$_i$ at the transition state, albeit less efficiently, in the absence of Arg56, partially offsetting the effect of the mutation.

Catalytic mechanism. The extensive structural work carried out here represents the most complete set of structures for an ATPPRT, allowing a catalytic mechanism to be proposed for the PaATPPRT-catalysed reaction (Scheme 2). Nucleophilic attack likely occurs from a resonance state of adenine in which N1 is negatively charged due to electron transfer from N6, an idea supported by density-functional theory calculations that indicate this natural resonance state represents 6.64% of the distribution of adenine resonance structures.[44] This resonance structure might be further stabilised by the proximity of N1 to the positively charged guanidinium group of Arg32. None of the crystal structures reported here showed a strong base near 6-NH$_2$ group, which suggests that deprotonation may occur only after N1-C1 bond formation and leaving group departure. The PRATP 6-NH$_2^+$ group has a pK_a of 8.5,[45] several log units lower than that of the 6-NH$_2$ group of ATP.[46] The PP$_i$ leaving group is stabilised at the transition state by H-bonds with Arg56, and probably departs the enzyme in a complex with a second Mg^{2+} ion.

A different kinetic mechanism may also be inferred from the set of structures presented here. HisG$_L$ ATPPRT's follow an ordered mechanism in which ATP is the first substrate to bind to, and PRATP the last product to dissociate from, the enzyme,[47] a proposal supported by crystal structures of HisG$_L$ showing catalytically viable complexes with either ATP or

PRATP,[8, 36, 48-49] but a dead-end binary complex with PPRP.[36] The structures of the various complexes of *Pa*HisG$_S$ and *Pa*ATPPRT suggest that HisG$_S$ ATPPRT's proceed by the same order of product dissociation, but the opposite order of substrate binding, with PRPP binding to the free enzyme, followed ATP binding. This is corroborated by the structure of *L. lactis* ATPPRT-PRPP binary complex.[19]

Scheme 2. Proposed catalytic mechanism for the *Pa*ATPPRT reaction.

Allosteric control of enzyme activity is a ubiquitous feature of metabolic and signalling pathways, and harnessing this control generates opportunities in drug design and biotechnology.[7, 12, 50] In large multiprotein complexes of key biosynthetic enzymes, elucidation of allosteric activation mechanisms can inform engineering of small subunits that capture full biosynthetic potential while reducing the protein synthesis burden of host cells.[51] Short-form ATPPRT's can be used in the industrial production of histidine as the catalytic activity of HisG$_S$ subunit is not subjected to inhibition by histidine. However, activity in the absence of HisZ is reduced.[15, 18] The work reported here provides a detailed structural picture of the interactions of activated and nonactivated *Pa*HisG$_S$ with substrates and products. These structures can serve as a framework for rational engineering of *Pa*HisG$_S$ towards increasing its catalytic activity. For instance, a combination of *in silico* mutations in *Pa*HisG$_S$ dimer interface and molecular dynamics simulations of the mutant *Pa*HisG$_S$ in complex with PRPP-ATP could be used to

identify variants which favour interaction between Arg56 and the PP_i leaving group, recapitulating the allosteric activation exerted by PaHisZ. Promising candidate PaHisG$_S$ mutants could then be produced and tested for improved catalytic properties.

SUPPORTING INFORMATION AVAILABLE

Materials and methods for the cloning, expression and purification of EcPRPPS, synthesis of D-ribose 5-phosphate, and synthesis and purification of PRATP, Figures S1 – S8, and Tables S1 – S3. This material is available free of charge via the internet at http://pubs.acs.org.

ABBREVIATIONS

ATP, adenosine 5′-triphosphate; ATPPRT, ATP phosphoribosyltransferase; PRPP, 5-phospho-α-D-ribosyl-1-pyrophosphate; PRATP, N^1-(5-phospho-β-D-ribosyl)-ATP; PP_i, inorganic pyrophosphate; HisG$_L$, long-form HisG; HisG$_S$, short-form HisG; PaHisG$_S$, $P.$ $arcticus$ HisG$_S$; PaATPPRT, $P.$ $arcticus$ ATPPRT; PaHisZ, $P.$ $arcticus$ HisZ; DTT, dithiothreitol; MtPPase, $Mycobacterium$ $tuberculosis$ inorganic pyrophosphatase; EcPRPPS, $E.$ $coli$ PRPP synthetase; MPD, 2-methyl-2,4-pentanediol; SEC, size-exclusion chromatography; MALS, multi-angle light scattering; LC-MS, liquid chromatography-mass spectrometry; ESI-MS, electrospray ionisation mass spectrometry; rmsd, root-mean square deviation; H-bond, hydrogen bond.

ACKOWLEDGEMENTS

REFERENCES AND FOOTNOTES

1.   Cho, Y.; Sharma, V.; Sacchettini, J. C., Crystal Structure of Atp Phosphoribosyltransferase from Mycobacterium Tuberculosis. *J. Biol. Chem.* 2003, 278, 8333-9.

2.   Lohkamp, B.; McDermott, G.; Campbell, S. A.; Coggins, J. R.; Lapthorn, A. J., The Structure of Escherichia Coli Atp-Phosphoribosyltransferase: Identification of Substrate Binding Sites and Mode of Amp Inhibition. *J. Mol. Biol.* 2004, 336, 131-44.

3.   Ames, B. N.; Martin, R. G.; Garry, B. J., The First Step of Histidine Biosynthesis. *J. Biol. Chem.* 1961, 236, 2019-26.

4.   Bell, R. M.; Koshland, D. E., Allosteric Properties of the First Enzyme of the Histidine Operon. *Bioorg. Chem.* 1971, 1, 409-423.

5.   Martin, R. G., The First Enzyme in Histidine Biosynthesis: The Nature of Feedback Inhibition by Histidine. *J. Biol. Chem.* 1963, 238, 257-268.

6.   Morton, D. P.; Parsons, S. M., Inhibition of Atp Phosphoribosyltransferase by Amp and Adp in the Absence and Presence of Histidine. *Arch. Biochem. Biophys.* 1977, 181, 643-8.

7.   Pedreno, S.; Pisco, J. P.; Larrouy-Maumus, G.; Kelly, G.; de Carvalho, L. P., Mechanism of Feedback Allosteric Inhibition of Atp Phosphoribosyltransferase. *Biochemistry* 2012, 51, 8027-38.

8.   Moggre, G. J.; Poulin, M. B.; Tyler, P. C.; Schramm, V. L.; Parker, E. J., Transition State Analysis of Adenosine Triphosphate Phosphoribosyltransferase. *ACS Chem. Biol.* 2017, 12, 2662-2670.

9.   Cho, Y.; Ioerger, T. R.; Sacchettini, J. C., Discovery of Novel Nitrobenzothiazole Inhibitors for Mycobacterium Tuberculosis Atp Phosphoribosyl Transferase (Hisg) through Virtual Screening. *J. Med. Chem.* 2008, 51, 5984-92.

10.   Ingle, R. A.; Mugford, S. T.; Rees, J. D.; Campbell, M. M.; Smith, J. A., Constitutively High Expression of the Histidine Biosynthetic Pathway Contributes to Nickel Tolerance in Hyperaccumulator Plants. *Plant Cell* 2005, 17, 2089-106.

11.   Wycisk, K.; Kim, E. J.; Schroeder, J. I.; Kramer, U., Enhancing the First Enzymatic Step in the Histidine Biosynthesis Pathway Increases the Free Histidine Pool and Nickel Tolerance in Arabidopsis Thaliana. *FEBS Lett.* 2004, 578, 128-34.

12.   Pisco, J. P.; de Chiara, C.; Pacholarz, K. J.; Garza-Garcia, A.; Ogrodowicz, R. W.; Walker, P. A.; Barran, P. E.; Smerdon, S. J.; de Carvalho, L. P. S., Uncoupling Conformational States from Activity in an Allosteric Enzyme. *Nat. Commun.* 2017, 8, 203.

13.   Mittelstadt, G.; Moggre, G. J.; Panjikar, S.; Nazmi, A. R.; Parker, E. J., Campylobacter Jejuni Adenosine Triphosphate Phosphoribosyltransferase Is an Active Hexamer That Is Allosterically Controlled by the Twisting of a Regulatory Tail. *Protein Sci.* 2016, 25, 1492-506.

14.   Pacholarz, K. J.; Burnley, R. J.; Jowitt, T. A.; Ordsmith, V.; Pisco, J. P.; Porrini, M.; Larrouy-Maumus, G.; Garlish, R. A.; Taylor, R. J.; de Carvalho, L. P. S.; Barran, P. E., Hybrid Mass Spectrometry Approaches to Determine How L-Histidine Feedback Regulates the Enzyme Mtatp-Phosphoribosyltransferase. *Structure* 2017, 25, 730-738.e4.

15.   Livingstone, E. K.; Mittelstadt, G.; Given, F. M.; Parker, E. J., Independent Catalysis of the Short Form Hisg from Lactococcus Lactis. *FEBS Lett.* 2016, 590, 2603-10.

16.   Sissler, M.; Delorme, C.; Bond, J.; Ehrlich, S. D.; Renault, P.; Francklyn, C., An Aminoacyl-Trna Synthetase Paralog with a Catalytic Role in Histidine Biosynthesis. *Proc. Natl. Acad. Sci. U S A* 1999, 96, 8985-90.

17.   Vega, M. C.; Zou, P.; Fernandez, F. J.; Murphy, G. E.; Sterner, R.; Popov, A.; Wilmanns, M., Regulation of the Hetero-Octameric Atp Phosphoribosyl Transferase Complex from Thermotoga Maritima by a Trna Synthetase-Like Subunit. *Mol. Microbiol.* 2005, 55, 675-86.

18.   Stroek, R.; Ge, Y.; Talbot, P. D.; Glok, M. K.; Bernas, K. E.; Thomson, C. M.; Gould, E. R.; Alphey, M. S.; Liu, H.; Florence, G. J.; Naismith, J. H.; da Silva, R. G., Kinetics and Structure of a Cold-Adapted Hetero-Octameric Atp Phosphoribosyltransferase. *Biochemistry* 2017, 56, 793-803.

19.   Champagne, K. S.; Sissler, M.; Larrabee, Y.; Doublie, S.; Francklyn, C. S., Activation of the Hetero-Octameric Atp Phosphoribosyl Transferase through Subunit Interface Rearrangement by a Trna Synthetase Paralog. *J. Biol. Chem.* 2005, 280, 34096-104.

20.   Champagne, K. S.; Sissler, M.; Larrabee, Y.; Doublie, S.; Francklyn, C. S., Activation of the Hetero-Octameric Atp Phosphoribosyl Transferase through Subunit Interface Rearrangement by a Trna Synthetase Paralog. *J. Biol. Chem.* 2005, 280, 34096-104.

21.   Kulis-Horn, R. K.; Persicke, M.; Kalinowski, J., Histidine Biosynthesis, Its Regulation and Biotechnological Application in Corynebacterium Glutamicum. *Microb. Biotechnol.* 2014, 7, 5-25.

22.   Kulis-Horn, R. K.; Persicke, M.; Kalinowski, J., Corynebacterium Glutamicum Atp-Phosphoribosyl Transferases Suitable for L-Histidine Production--Strategies for the Elimination of Feedback Inhibition. *J. Biotechnol.* 2015, 206, 26-37.

23.   Schendzielorz, G.; Dippong, M.; Grunberger, A.; Kohlheyer, D.; Yoshida, A.; Binder, S.; Nishiyama, C.; Nishiyama, M.; Bott, M.; Eggeling, L., Taking Control over Control: Use of Product Sensing in Single Cells to Remove Flux Control at Key Enzymes in Biosynthesis Pathways. *ACS Synth. Biol.* 2014, 3, 21-9.

24.   Becker, J.; Wittmann, C., Systems and Synthetic Metabolic Engineering for Amino Acid Production - the Heartbeat of Industrial Strain Development. *Curr. Opin. Biotechnol.* 2012, 23, 718-26.

25.   Becker, J.; Zelder, O.; Hafner, S.; Schroder, H.; Wittmann, C., From Zero to Hero--Design-Based Systems Metabolic Engineering of Corynebacterium Glutamicum for L-Lysine Production. *Metab. Eng.* 2011, 13, 159-68.

26.   Battye, T. G.; Kontogiannis, L.; Johnson, O.; Powell, H. R.; Leslie, A. G., Imosflm: A New Graphical Interface for Diffraction-Image Processing with Mosflm. *Acta Crystallogr D Biol. Crystallogr.* 2011, 67, 271-81.

27.   Winter, G., Xia2: An Expert System for Macromolecular Crystallography Data Reduction. *J. Appl. Crystallogr.* 2010, 43, 186-190.

28.   Kabsch, W., Xds. *Acta Crystallogr D Biol Crystallogr* 2010, 66, 125-132.

29.   Vagin, A.; Teplyakov, A., Molrep: An Automated Program for Molecular Replacement. *J. Appl. Crystallogr.* 1997, 30, 1022-1025.

30.   Emsley, P.; Cowtan, K., Coot: Model-Building Tools for Molecular Graphics. *Acta Crystallogr. D Biol. Crystallogr.* 2004, 60, 2126-32.

31.   Murshudov, G. N.; Vagin, A. A.; Dodson, E. J., Refinement of Macromolecular Structures by the Maximum-Likelihood Method. *Acta Crystallogr. D. Biol. Crystallogr.* 1997, 53, 240-55.

32.   Long, F.; Nicholls, R. A.; Emsley, P.; Graaeulis, S.; Merkys, A.; Vaitkus, A.; Murshudov, G. N., Acedrg: A Stereochemical Description Generator for Ligands. *Acta Crystallogr. D Struct. Biol.* 2017, 73, 112-122.

33.   Schuttelkopf, A. W.; van Aalten, D. M., Prodrg: A Tool for High-Throughput Crystallography of Protein-Ligand Complexes. *Acta Crystallogr. D Biol. Crystallogr.* 2004, 60, 1355-63.

34.   Liu, H.; Naismith, J. H., An Efficient One-Step Site-Directed Deletion, Insertion, Single and Multiple-Site Plasmid Mutagenesis Protocol. *BMC Biotechnol.* 2008, 8, 91.

35.   Champagne, K. S.; Piscitelli, E.; Francklyn, C. S., Substrate Recognition by the Hetero-Octameric Atp Phosphoribosyltransferase from *Lactococcus Lactis*. *Biochemistry* 2006, 45, 14933-43.

36.   Mittelstadt, G.; Jiao, W.; Livingstone, E. K.; Moggre, G. J.; Nazmi, A. R.; Parker, E. J., A Dimeric Catalytic Core Relates the Short and Long Forms of Atp-Phosphoribosyltransferase. *Biochem. J.* 2018, 475, 247-260.

37.   Burgos, E. S.; Vetticatt, M. J.; Schramm, V. L., Recycling Nicotinamide. The Transition-State Structure of Human Nicotinamide Phosphoribosyltransferase. *J. Am. Chem. Soc.* 2013, 135, 3485-93.

38.   Guthrie, R. D.; Jencks, W. P., Iupac Recommendations for the Representation of Reaction Mechanisms. *Acc. Chem. Res.* 1989, 22, 343-349.

39.   In Iupac recommendation for reaction mechanism nomenclature (See Reference 36), A_ND_N describes an associative nucleophilic substitution reaction mechanism where the electrophile is partially bonded to both incoming nucleophile and departing leaving group at the transition state. $D_N*A_N^{\ddagger}$ describes a dissociative nucleophilic substitution reaction mechanism where the leaving group departs to form an intermediate, and the highest-energy transition state is the one for subsequent nucleophilic attack to the intermediate.

40.   Barrozo, A.; Duarte, F.; Bauer, P.; Carvalho, A. T.; Kamerlin, S. C., Cooperative Electrostatic Interactions Drive Functional Evolution in the Alkaline Phosphatase Superfamily. *J. Am. Chem. Soc.* 2015, 137, 9061-76.

41.   Pabis, A.; Kamerlin, S. C., Promiscuity and Electrostatic Flexibility in the Alkaline Phosphatase Superfamily. *Curr. Opin. Struct. Biol.* 2016, 37, 14-21.

42.   Hammes, G. G.; Benkovic, S. J.; Hammes-Schiffer, S., Flexibility, Diversity, and Cooperativity: Pillars of Enzyme Catalysis. *Biochemistry* 2011, 50, 10422-10430.

43.   Pabis, A.; Risso, V. A.; Sanchez-Ruiz, J. M.; Kamerlin, S. C., Cooperativity and Flexibility in Enzyme Evolution. *Curr. Opin. Struct. Biol.* 2018, 48, 83-92.

44.   Sun, G.; Nicklaus, M. C., Natural Resonance Structures and Aromaticity of the Nucleobases. *Theor. Chem. Acc.* 2007, 117, 323-332.

45.   Smith, D. W.; Ames, B. N., Phosphoribosyladenosine Monophosphate, an Intermediate in Histidine Biosynthesis. *J. Biol. Chem.* 1965, 240, 3056-63.

46.   Añorbe, M. G.; Lüth, M. S.; Roitzsch, M.; Cerdà, M. M.; Lax, P.; Kampf, G.; Sigel, H.; Lippert, B., Perturbation of the Nh2 Pka Value of Adenine in Platinum(Ii) Complexes: Distinct Stereochemical Internucleobase Effects. *Chemistry* 2004, 10, 1046-1057.

47.   Morton, D. P.; Parsons, S. M., Biosynthetic Direction Substrate Kinetics and Product Inhibition Studies on the First Enzyme of Histidine Biosynthesis, Adenosine Triphosphate Phosphoribosyltransferase. *Arch. Biochem. Biophys.* 1976, 175, 677-86.

48.   Mittelstadt, G.; Moggre, G. J.; Panjikar, S.; Nazmi, A. R.; Parker, E. J., *Campylobacter Jejuni* Adenosine Triphosphate Phosphoribosyltransferase Is an Active Hexamer That Is Allosterically Controlled by the Twisting of a Regulatory Tail. *Protein Sci.* 2016, 25, 1492-506.

49.   Lohkamp, B.; McDermott, G.; Campbell, S. A.; Coggins, J. R.; Lapthorn, A. J., The Structure of *Escherichia Coli* Atp-Phosphoribosyltransferase: Identification of Substrate Binding Sites and Mode of Amp Inhibition. *J. Mol. Biol.* 2004, 336, 131-144.

50.   Cramer, J. T.; Führing, J. I.; Baruch, P.; Brütting, C.; Knölker, H.-J.; Gerardy-Schahn, R.; Fedorov, R., Decoding Allosteric Networks in Biocatalysts: Rational Approach to Therapies and Biotechnologies. *ACS Catal.* 2018, 2683-2692.

51.   Buller, A. R.; Brinkmann-Chen, S.; Romney, D. K.; Herger, M.; Murciano-Calles, J.; Arnold, F. H., Directed Evolution of the Tryptophan Synthase Beta-Subunit for Stand-Alone Function Recapitulates Allosteric Activation. *Proc. Natl. Acad. Sci. U S A* 2015, 112, 14599-604.